Middle East Journal of Applied Sciences
Volume: 14 | Issue: 03| July – Sept. | 2024

EISSN: 2706 -7947 ISSN: 2077- 4613
DOI: 10.36632/mejas/2024.14.3.28
Journal homepage: www.curresweb.com
Pages: 353-371

Petrophysical Characteristics of the Nukhul Clastic Formation in The Southern Province of the Gulf of Suez, Egypt

Emad A. Abd El Aziz and Mohamed M. Gomaa

Geophysical Sciences Dept., Geophysical exploration Lab., National Research Centre (NRC), 33 El-Buhouth St., 12622 Dokki, Giza, Egypt.

Received: 07 May 2024 **Accepted:** 15 July 2024 **Published:** 30 July 2024

ABSTRACT

The Nukhul reservoir (Lower Miocene) representing the most prolific target in the Gulf of Suez that deposited during the early stage of the Gulf rift with gross thickness reach to 140 ft. The lithofacies of the Nukhul reservoir in the study area could be differentiated into two facies 1) Shaly carbonates that is represented by zones 1and 3 which reflecting non reservoir intervals, 2) sandy facies that is represented by zones 2 and 4 which reflect a small pay zones intervals localized mainly within the sandstone beds. The present work is achieved by analysis of the well logs and core samples data sets. The petrophysical analysis of the detected lithofacies types of Nukhul reservoirs reflect that sandy facies (zone 2 and 4) show that the shale content has minor amount by a wetted average values ranges (4% - 5%), whereas the effective porosity is recorded with high values (19 % - 20%) , indicating a reversible trend between shale and porosity. The average permeability ranges from 111.4 md to 245.5 md. The water saturation value ranged between 31 % and 21%. The hydrocarbon saturation is represented with average 69 % and 79 %; The pay zones yield 14 ft and 10 ft for zones 2 and 4 respectively. The sandy intervals (zone 2 and 4) are characterized by high gas records during drilling. Conversely, the shaly carbonates facies (zones 1 and 3) reflected the bad petrophysical properties. Petrophysical characters of Nukhul reservoir including Vsh, Phie, Sw, So and net pay thickness are represented vertically by constructing the litho-saturation crossplot.

Keywords: Nukhul reservoir, petrophysical analysis, net pay, microfacies, Gulf of Suez.

1. Introduction

One of the ancient oil regions is the Suez Gulf. With eighty production oil fields spread over the Middle East and Africa, it is the maximum active oil-rift reservoir (Bosworth and McClay 2001; Alsharhan 2003). It covers an area of 19,000 km^2 and its widths in the north and south vary from 50 to 90 km (Schlumberger 1995; El Nady *et al.,* 2016; Radwan 2021; Radwan and Sen 2021). Suez Gulf (NW-SE) is a subsidence area defined as somewhat arcuate and renewed taphrogenic depression (Gomaa 2009, Gomaa 2013, Gomaa 2021a, 2021b, 2021c). Suez Gulf having two fault systems: one NW-SE (Clysmic trend) and one NE-SW (Aqaba trend). Rifting period at Suez Gulf began at early Paleozoic and continued until the later to middle Tertiary. Suez Gulf is impacted by five tectonic events, which are listed from bottom to top as pan-African, Hercynian, Neo-Tethyan, Syrian Arc, and Suez Gulf (Radwan *et al.,* 2021b). The structural context of Suez Gulf exerts more influence over the depositional environment, sedimentation patterns, hydrocarbon buildup, and entrapment (Sultan 2002; Leila and Moscariello 2018; Moustafa and Khalil 2020). In addition to sedimentary facies, source and seal rock, the synrift sediments of Suez Gulf include the majority of hydrocarbon accumulations. The synrift Miocene sediments occupied 60% of Egypt's oil reserves, with the Nubia Formation accounting for the other 40% (Peijs *et al.,* 2012; Chowdhary and Taha 1987).

Most hydrocarbon accumulations in the investigated Rabeh field of the Southern Suez Gulf are contained mostly within synrift Miocene clastic strata (Fig. 1). The most plentiful oil deposits in the

Corresponding Author: Mohamed M. Gomaa, Geophysical Sciences Dept., Geophysical exploration Lab., National Research Centre (NRC), 33 El-Buhouth St., 12622 Dokki, Giza, Egypt.
E-mail: mmmsgomaa@yahoo.com

Suez Gulf province therefore occur in the Miocene synrift sedimentary strata. Nukhul Formation (Lower Miocene) is the maximum prolific formation at Suez Gulf, depositing during early stages of Gulf-Rift and reaching a gross thickness of 140 feet. More than 15 fields in Suez Gulf generate hydrocarbons from the Nukhul Formation. The principal discovered lithofacies of the examined Nukhul Formation include evaporites, carbonates, shale, marl, and sandstone with respectable thicknesses up to 313 ft (Fig. 2). In the research region, the Nukhul Formation is divided into two facies: evaporitic and clastic.

The current study focuses solely on the clasticsfacies and their relationship to petrophysical characteristics (Ammar *et al.,* 2021, Saoudi and Khalil 1986; Sarhan 2020; Sarhan 2021; Temraz and Dypvik 2018, Sherif 2023). This work offers a path to analyze the petrophysical parameters of the examined Nukhul Formation and distinguish it into various assemblage groups based on petrophysical characteristics and microfacies analysis, followed by statistical analysis of avialble data. This is a trail to assess the models that rationalized the various petrophysical parameters and hydrocarbon potentialities of the Nukhul reservoirs within the Rabeh oil field.

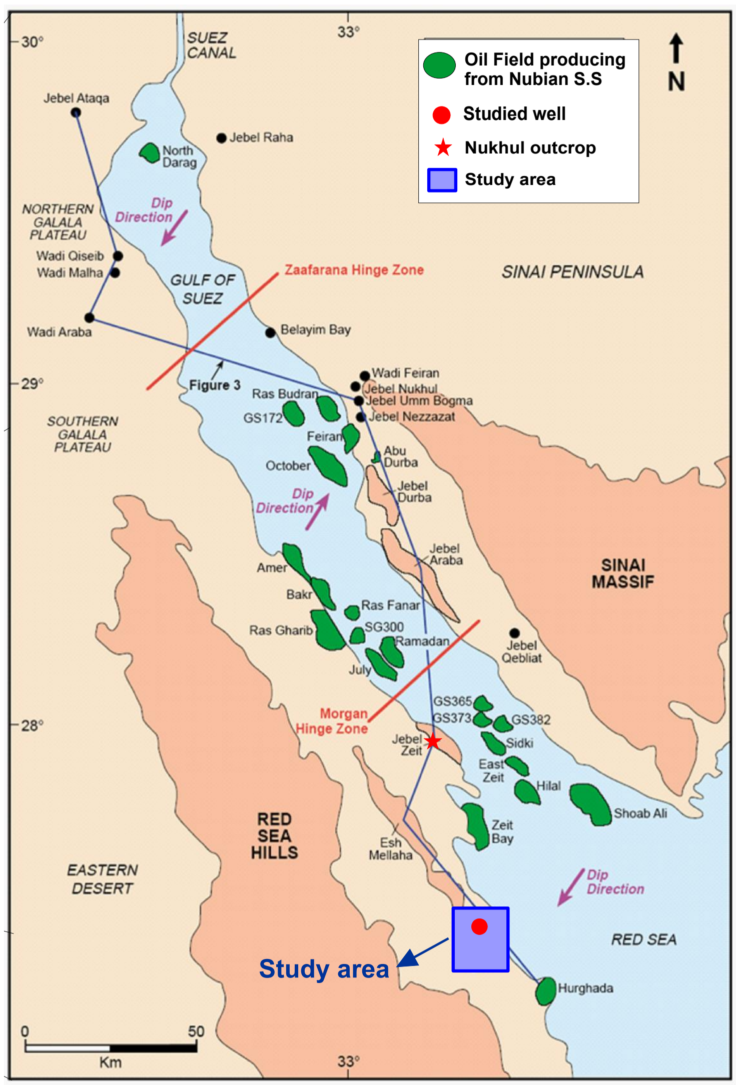

Fig. 1: Location map showing thestudy area, studied well and Nukhul formation outcrop, Southern Gulf of Suez, Egypt (Modified afterSarhan and Salah 1997).

2. Geologic setting

2.1. Tectonic and structural background of Suez Gulf

Research area occurs in Suez Gulf area, which has direct control over sedimentation patterns (Fig.2). Suez Gulf is characterized as a rift graben molded by tectonic events that began in the Oligocene and persisted into the Post-Miocene period. These tectonic motions cause regional subsidence, which is related with a large transgression in the lower to middle Miocene. The rift is composed of two orthogonal normal fault classifications: one parallel to the Gulf of Aqaba and oriented NE-SW (Aqaba trend); the other is directed NW-SE (Clysmic trend) and parallel to the Suez Gulf. These two fault systems produce little slanted blocks of grabens and half-grabens separated by horses. Suez Gulf is separated into three dip provinces based on fault polarity (northern, southern, and center). Northern and southern dip provinces are distinguished by the fact that their normal faults mainly dip toward the northeast and their layers commonly dip toward the southwest, whereas the normal faults of central dip provinces frequently dip to the southwest and their strata commonly dip toward the northeast. The rift-transverse lodging zones distinguish between dip provinces (Omar *et al.,* 1989; Moustafa 1997).

Suez Gulf rift is thought to represent the right lateral component of two complimentary shear fractures: Suez Gulf and Aqaba Gulf. Suez Gulf (clysmic gulf) is defined geomorphologically as a taphrogenic depression going NW-SE, renewed and somewhat arcuate. During extensional faulting, non-clysmic faults exist in multiple regions of the rift, known as cross faults. Clysmic fault propagation might be inhibited and moved laterally along cross faults (Colleta *et al.,* 1988; EGPC 1996; Alsharhan 2003). The primary reported tectonic occurrences in Suez Gulf from bottom to top are the pan-African, Hercynian, Neo-Tethyan, Syrian Arc, and Suez Gulf rifting (Said 1990). The interaction of rift parallel faults, cross faults, shear zones, and the plunging direction of basement blocks were the primary factors controlling the localization of the Miocene sediment entrapment system (Robson 1971; Khalil and Mesheref 1988; Alsharhan 2003; Khalil and McCaly 2004; Saoudi *et al.,* 2014; Abd El Gawad 2016).

2.2. Suez Gulf General stratigraphic setting

Suez's Gulf sediment distribution is mostly determined by its tectonic context. Suez Gulf source rocks are selected for their rapid sedimentation rates, organic matter content enrichment, and considerable thickness (Sellwood and Netherwood 1984). The carbonate series were deposited along the high sides of the uplifted fault blocks and the Suez reservoir edges. The thick calcareous and impending evaporatic series is deposited along the Gulf reservoir's edges. The heaviest salt development occurs along the Suez rift and the Red Sea. The evaporite series in the Gulf province are regarded as the finest cap rock for oil accumulation (Mostafa 1996, EGPC 1996). The Miocene sediments are distinguished by fast facies change caused by rapid subsidence, which led to the deposit of a thick succession of evaporates, clastics, and carbonates. The lower Miocene sediments are unconformably deposited on the slanted fault blocks of the Pre Miocene Formations.

The stratigraphic portion of Suez Gulf rift was divided into post-rift, syn-rift, and pre-rift phases (Fig. 3). The synrift mega series of Suez Gulf subdivided into two sedimentary groups: Gharandal (clastic phases), which is connected to the Nukhul, and the RasMalaab Group (evaporites phases).(Robson 1971; Garfunkel and Bartov 1977; Evans 1988; Evans 1990;Abul-Nasr 1990; El-Ghali *et al.,* 2013; Zaid 2013;Abd El Aziz and Gomaa 2022a; Abd El Aziz and Gomaa 2022b, Gomaa and Abd El Aziz 2024).

The peripheral facies of the synrift Miocene phase is mostly composed of five formations, aranged from top to bottom as Zeit sand, Belayim, Kareem, Rudies, and Nukhul carbonates. The Zeit and South Gharib Formations are from the upper Miocene, the Belayim and Kareem Formations from the middle Miocene, and the Gharandal and Nukhul Formations from the lower Miocene. The Nukhul Formation was deposited under alluvial fan, lacustrine, fluvial, lagoonal, shallow-marine, and potentially deep marine depositional conditions. It is unconformably overlain by the Rudies Formation and unconformably underlain by the Theibes Formation (McClay *et al.,* 1998; Temraz and Dypvik 2018). The brown limestone deposit most likely produced oil during the Middle Miocene and Pliocene epochs. The hydrocarbon migration occurs up dip and along fault migration channels (Corex 2009; Alsharhan 2003; Abd El Aziz and Gomaa 2022). Outcrop of the examined formation has emerged in Gebel el Zeit, close to the research area. This outcrop comprises the uplifted section of early sedimentary synrift strata in Suez Gulf rift, which are mostly made up of evaporites, limestones, marl, shale, sandstones, and conglomerates (Temraz and Dypvik 2018; Sarhan 2021).

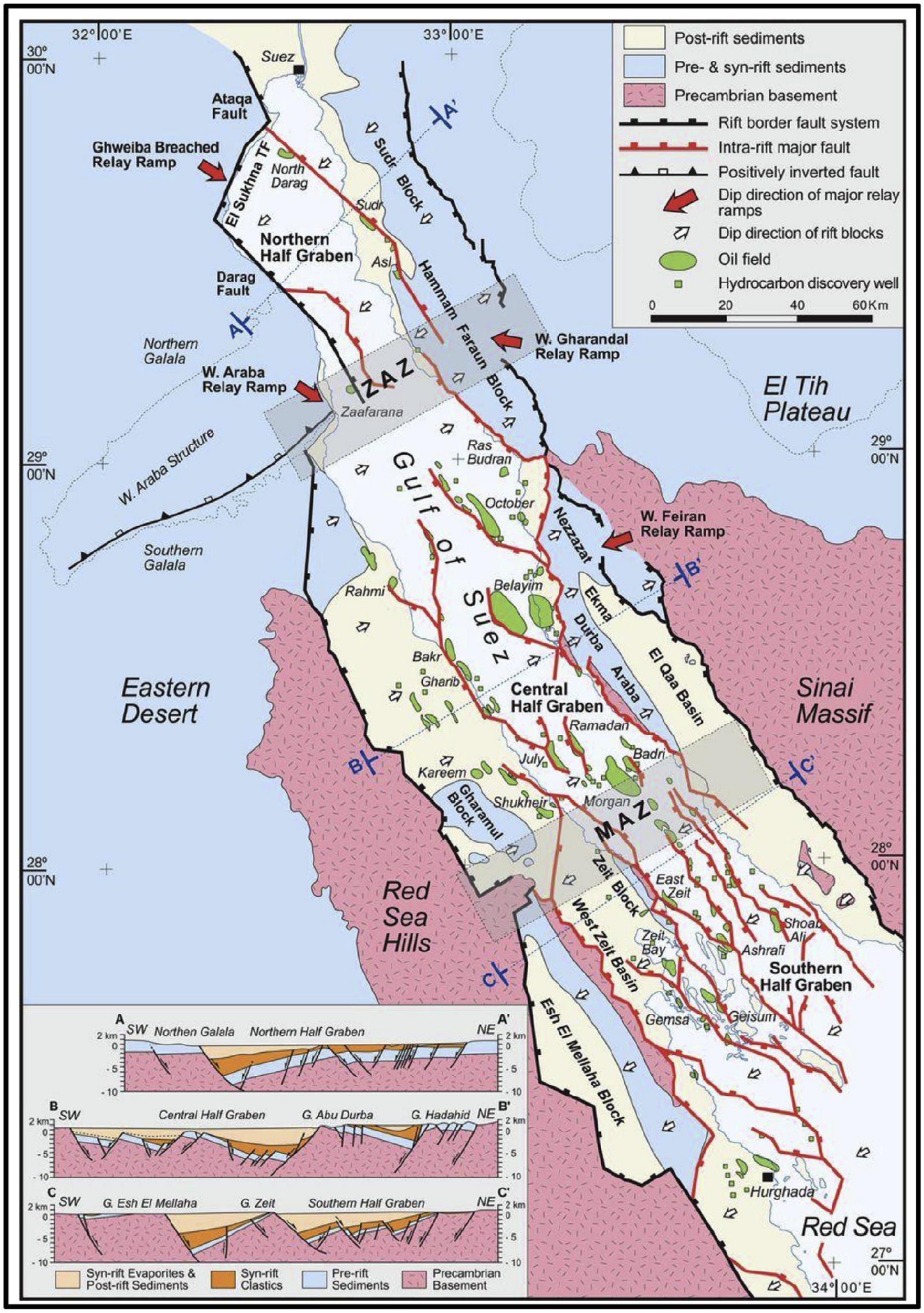

Fig. 2: Structural setting of the Gulf of Suez, Egypt. showing different dip directions of three provinces (after Moustafa and Khalil, 2016).

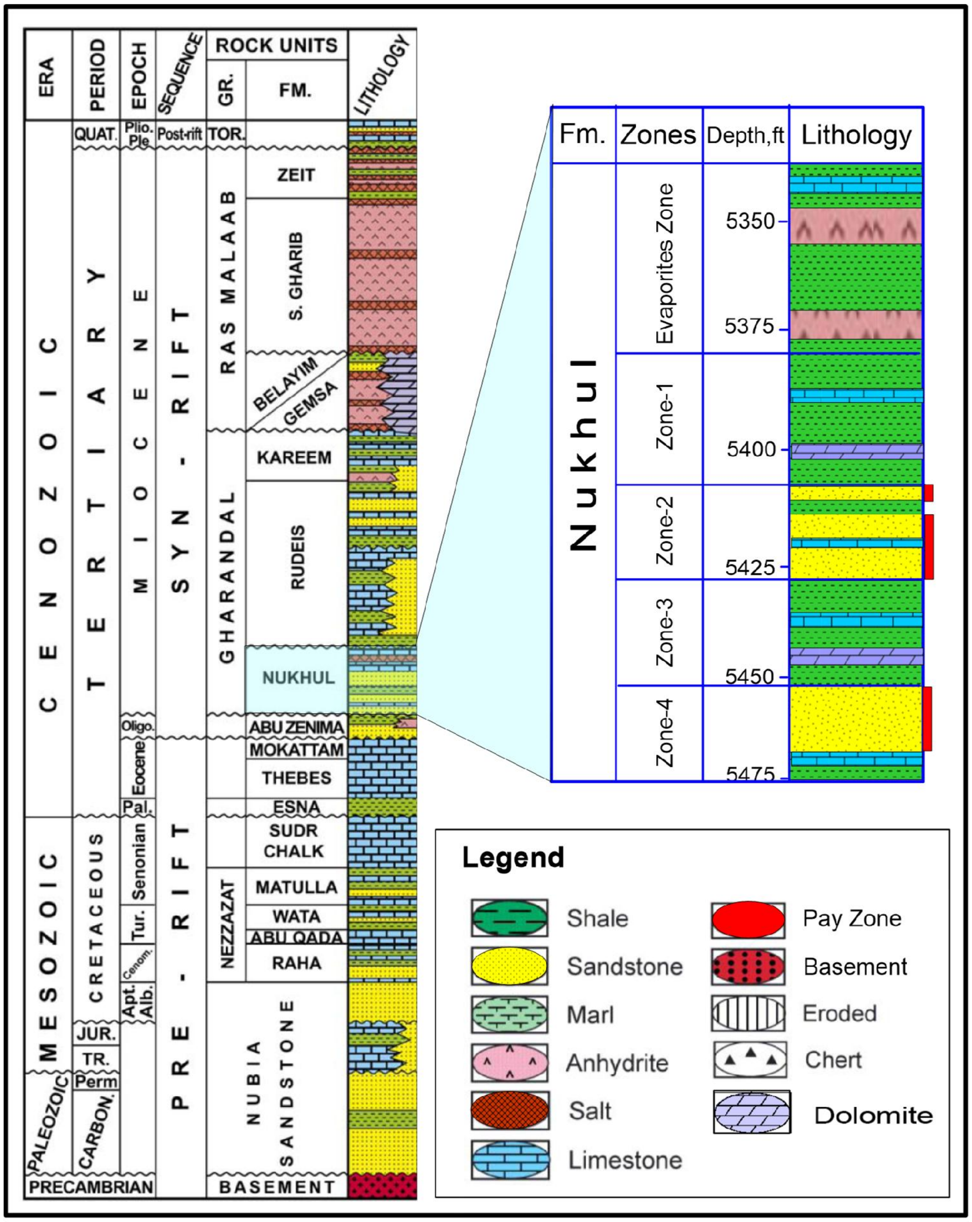

Fig. 3: Generalized stratigraphic column of Suez Gulf with detailed SynriftMiocene lithology components of the Nukhul Formation (Modified after Darwish and El Araby 1993, Saoudi *et. al.,* 2014).

3. Data sets and Methodology

Petrophysical properties of Nukhul Formation at Rabeh field are evaluated using various suites of wire-line log data, including caliper, neutron, density, sonic, photoelectric absorption factor (Pe), and resistivity logs (MSF), shallow (LLS) and deep (LLD) in the las file format, as well as drill cutting samples covering the majority of whole formation depths. The quantitative examination of the Nukhul reservoir is carried out using an interactive petrophysics program (IP). A cross plot of (NPHI) versus (RHOB) was created for matrix identification (Schlumberger 1998). Water resistivity (Rw) was visually calculated using the Picket Plot (Archie 1942; Pickett 1973).

$$Rt = R_W \phi^{-m} \quad (1)$$

EISSN: 2706 -7947 ISSN: 2077- 4613 DOI: 10.36632/mejas/2024.14.3.28

Where Rt = true resistivity of the formation (Ohm m.), ϕ = Porosity (Decimal), R_W = resistivity of water (Ohm m.), Sw is the water saturation, a proportionality constant, n saturation exponent and m = cementation factor. For consolidated sandstones m(cementation exponent)=1.7,a (tortuosity) = 0.81, and n(saturation exponent) = 2.0. For carbonates, a =1.0 and m= n=2.0.

$$S_W = \sqrt[n]{\frac{aR_W}{\phi^m R_T}} \qquad (2)$$

Where R_T is the true formation resistivity (Ohm m.), a proportionality constant , S_W water saturation (Decimal), and R_W = resistivity of water (Ohm m.). The hydrocarbon saturation (S_O) achieved from the following relation.

$$S_O = 1 - S_W \qquad (3)$$

Shale content levels were determined using five indicators: gamma ray, neutron, resistivity, neutron-resistivity, and neutron-density logs. Average values of variables are likely to be fairly near to the true shale volume. The corrected effective porosity (ϕ_e) is largely determined by the combination of density and neutron logs after performing adjustments using Schlumberger's (1972) equation.

$$\phi_e = \frac{2\phi_{NC} + 7\phi_{DC}}{9}\left(1 - 0.10S_{hr}\right) \qquad (4)$$

Where ϕ_{NC} is the corrected neutron porosity; ϕ_{DC} is the corrected density-derived porosity and S_{hr} is the residual hydrocarbon saturation. Cut off used in pay zone evaluation is the porosity $\geq$ 7%, water saturation $\leq$ 50% and volume of shale $\leq$35 %.

Prior to thin section production, chosen drill cutting samples were examined using scanning electron microscopy. The specimens were attached to aluminum stubs with carbon-based, electrically conductive double-sided adhesive tape. The drill chip samples were prepared for thin section description by being impregnated with blue epoxy to determine porosity and dyed with alizarin red to distinguish between calcite and dolomite. The thin section samples were examined using a polarizing microscope. Limestone has been described and named after Dunham (1962). Drill cutting samples were taken from RE-8X well, which enriched the distinctive facies investigations that are now being conducted.

4. Results and Discussion

The evaluation of the Nukhul reservoir may be discussed vertically using variable relationship cross plots and litho-saturation cross plots, after which all metrics for this studied section are combined. Furthermore, petrographical sample descriptions are required to accomplish the qualities of researched reservoir rock types in order to estimate the many aspects impacting hydrocarbon occurrences in the study region, as briefly stated in the following:

4.1. Reservoir rock characterization

4.1.1. Petrographical description

The Nukhul reservoir is composed of siliciclastic sandstone and shaly carbonate deposits. The sandy facies is defined as quartz arenite, fine to coarse grained, sub-rounded to subangular, moderate to well-sorted grains, good grain textural maturity, mostly mono-crystalline with few polycrystalline grains, concave-convex grained contacts, and extremely porous. These holes are partially blocked by pore-filling evaporites, dolomite, and minor glauconite. The point-counted porosity values vary from 2% to 24% by volume (Fig. 4 A and B). Disseminated dolomite is extensively used as a cementing material in the examined reservoir. The shaly carbonate is represented by dolomitic wackestone and extremely fine crystalline, tight dolomite composed primarily of vugs (yellow arrows), with a few polycrystalline and mono-crystalline quartz grains (blue arrows) (Fig. 4 C and D).

EISSN: 2706 -7947 ISSN: 2077- 4613 ***DOI: 10.36632/mejas/2024.14.3.28***

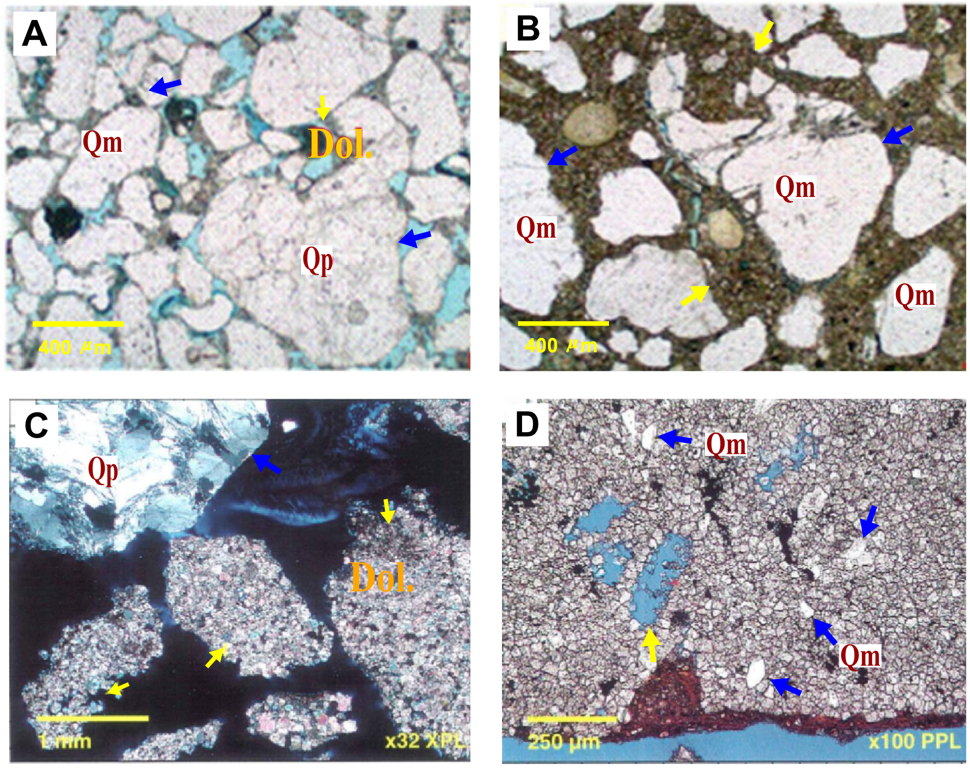

Fig. 4: Photomicrographs representing the studied NukhulFormation of the study area: A; Quartz arenitewith sutured polycrystalline grains (Qp), highly porous, and slightly cemented with dolomite, grains (Qp) are varies in size from very fine to pebbly grains, with sub angular to sub-rounded, and moderately to well-sorted grains, B; Sandstone with partially dolomitized quartz grains, Quartz grains are predominantly mono-crystalline (Qm), C; Very fine crystalline, tight dolomite porosity is compressed mainly of vugs (yellow arrows), poly crystalline quartz (blue arrows). D; Dolowacke stone with scattered mono-crystalline quartz grains (blue arrows).

4.1.2. Lithology identification by density-neutron cross plot

A crossplot between bulk density (RHOB) and neutron porosity (NPHI) was generated for matrix identification (Schlumberger 1998). The density-neutron cross plots show that the examined reservoir has a typical two thin layers of sandy facies intervals (zones 2 and 4) confined between depths 5410 - 5426 ft and 5449-5460 ft, respectively (Fig. 5). Another ensemble depicted point represents the carbonate facies intervals (zones 1 and 3), which are confined between depths 5391-5410 ft and 5426-5449 ft, respectively (Figs. 6).

The cross plots show that the sandy facies (zones 2 and 4) are mostly closed around sandstone trend, with a few points pointing towards matrix carbonates with ρ bulk ranging from 2.27 gm/cc to 2.57 gm/cc, with an average of 2.36 gm/cc. The shaly carbonates facies intervals are mostly closed around carbonates and shale trends with ρ bulk ranging from 2.44 gm/cc to 2.60 gm/cc, with an average of 2.50 gm/cc.

Middle East J. Appl. Sci., 14(3): 353-371, 2024
EISSN: 2706 -7947 ISSN: 2077- 4613 *DOI: 10.36632/mejas/2024.14.3.28*

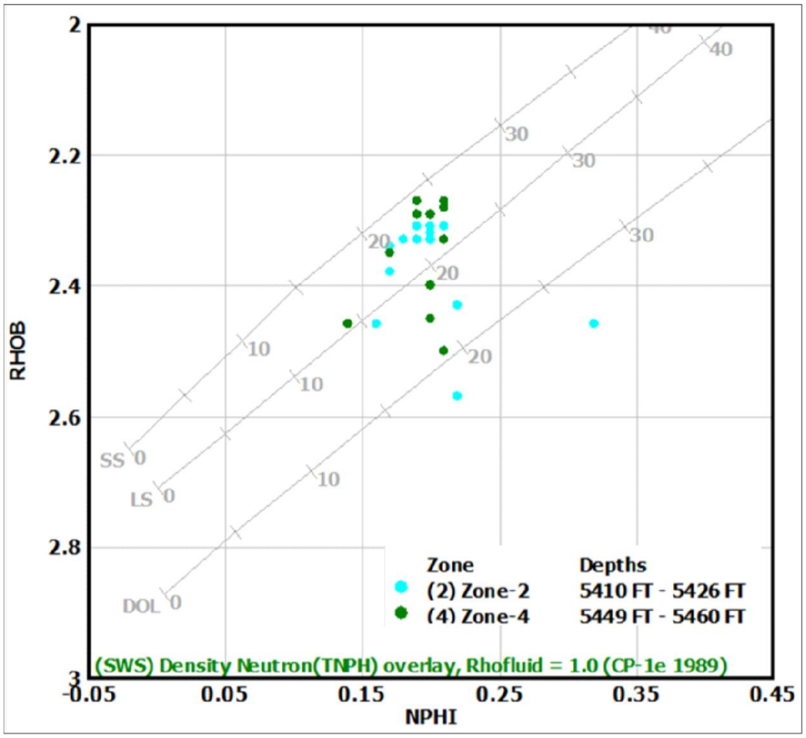

Fig. 5: Neutron - density cross plot for Nukhul reservoir (Zone 2and 4) in the study area, Southern Gulf of Suez, Egypt.

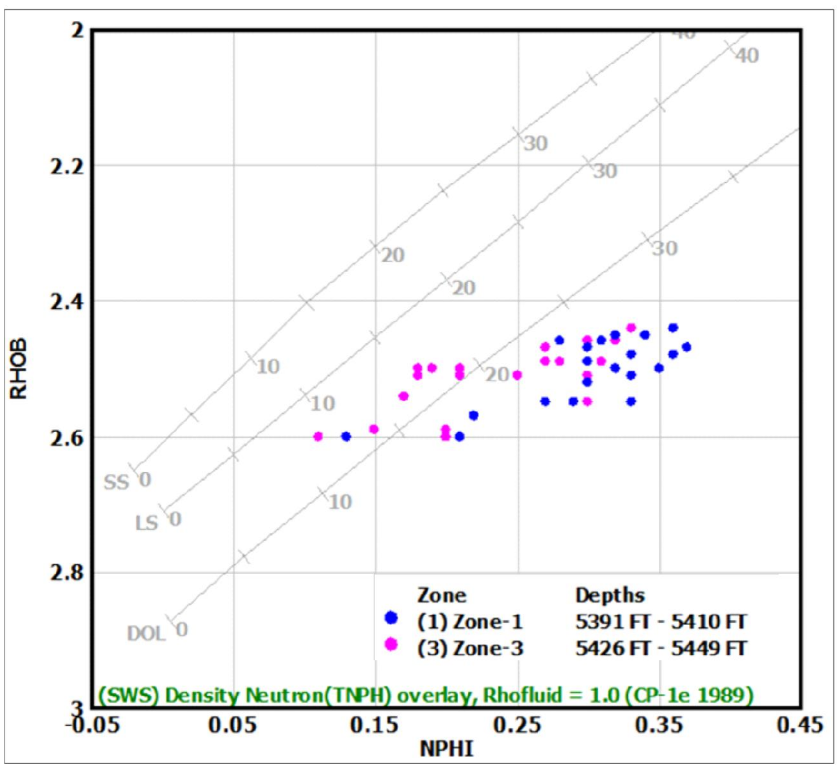

Fig. 6: Neutron - density cross plot for non-reservoirrock units (Zone 1 and 3) of Nukhul Formation in the study area, Southern Gulf of Suez, Egypt.

Middle East J. Appl. Sci., 14(3): 353-371, 2024
EISSN: 2706 -7947 ISSN: 2077- 4613 DOI: 10.36632/mejas/2024.14.3.28

4.1.3. Mineral identification by M-N cross plot

M-N cross plot shows that all plotted sites of sandy facies are confined mostly around quartz minerals, with a few points extending to calcite and dolomite regions, particularly in zone 2 (Fig. 7). Whereas, all plotted points of the shaly carbonates facies are confined primarily around shale regions, with a few points existed around anhydrite and dolomite trends (Figs. 8).

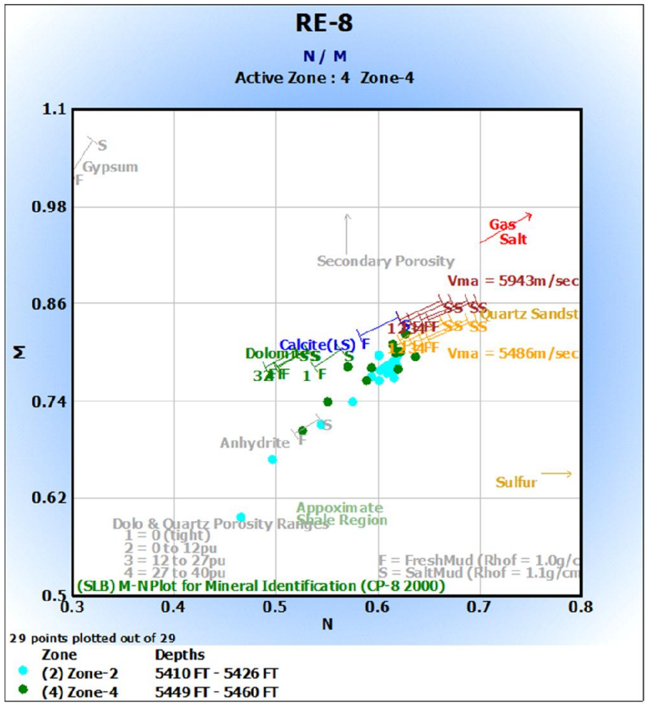

Fig. 7: M-N Cross plot for Nukhulreservoir (Zone 2 and 4) in the study area, SouthernGulf of Suez, Egypt.

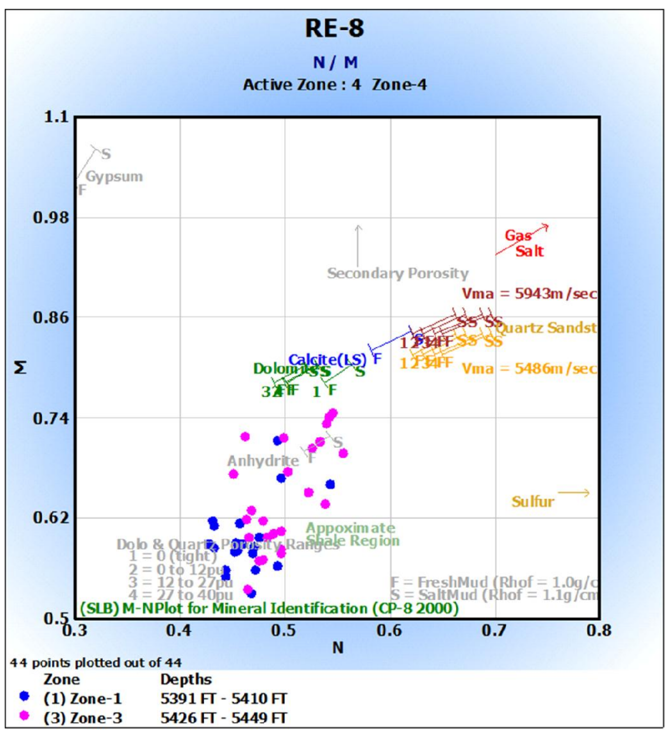

Fig. 8: M-N Cross plot for non-reservoirrock units (Zone 1 and 3) of Nukhul Formation in the study area, Southern Gulf of Suez, Egypt.

4.2. The wire-line logs analysis

The Nukhul reservoir (target of the study) is mostly made up of two narrow pay zone intervals localized mainly in the sandy intervals (zone 2 and 4) between depths 5410- 5426 ft and 5449-5460 ft, respectively, enclosed between shaly carbonate facies intervals (zone 1and 3) existed at depths 5391-5410ft and 5426 - 5449 ft, respectively, representing non-reservoir zones. The ditch sample revealed that the two sandy facies (zones 2 and 4) were described as colorless, yellow white, or off white, loose, moderate to coarse grained, sub-angular to sub-round with calcareous cement, moderately sorted, and had good textural maturity. which remarkably assigned by excellent evidence of oil shows and a high recording of gas readings opposing these zones (Fig. 9, Track 9).

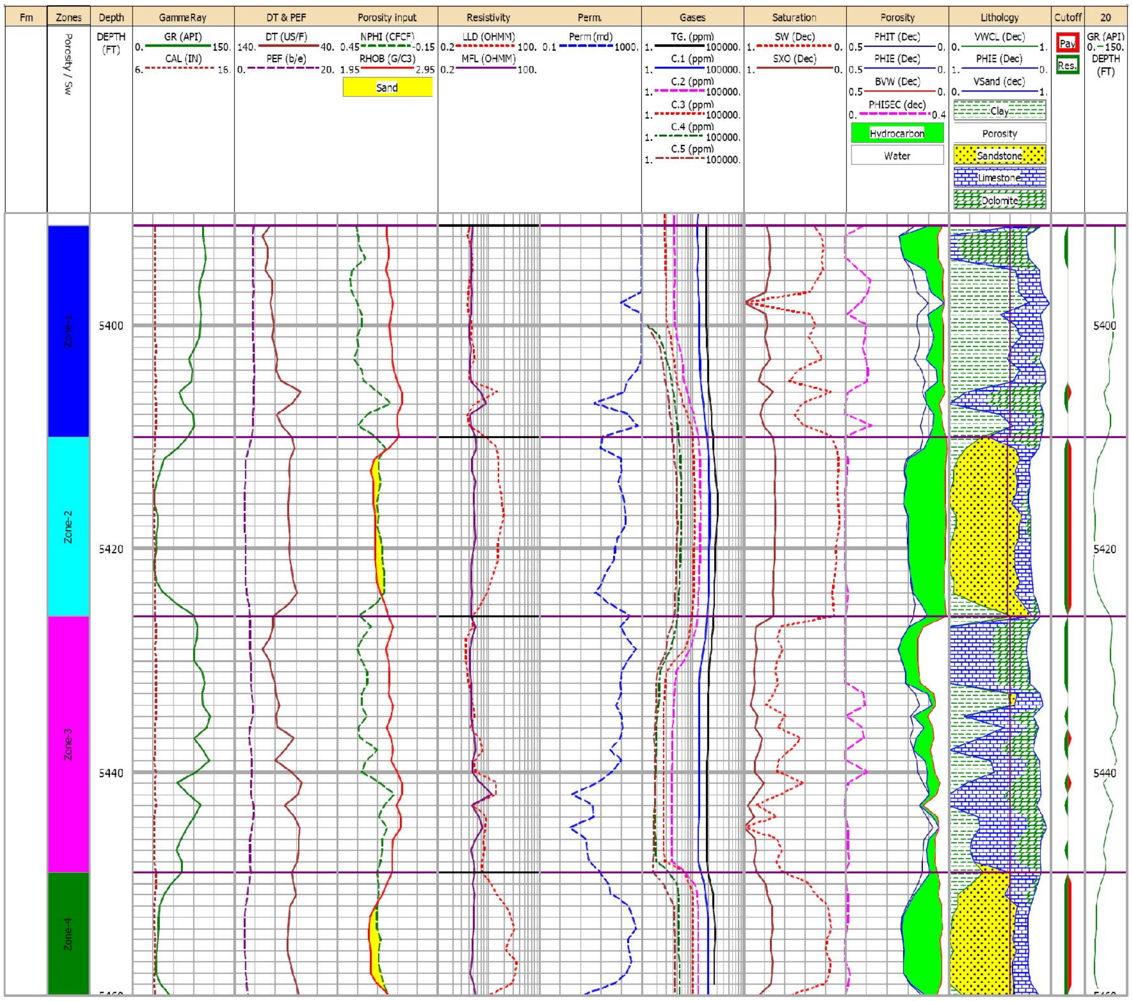

Fig. 9: Litho-saturation cross plot of Nuhkul Formation, RE-8X well, Southern Gulf of Suez, Egypt.

The petrophysical analysis of the studied interval is represented vertically by construction of litho-saturation cross plot (Computer Processing Interpretation, CPI) for the studied wells (Fig. 9), which indicated that the wetted average of the shale content (zone 2 and 4) is oscillated with minor amount along the studied section by an average amount ranged between 4% - 5% at zones 2 and 4, respectively. The effective porosity is observed to be high at zones 2 and 4 with 19 % and 20 % respectively. This is due to low shale content and low degree of diagenetic effect which confirmed by petrographical invetigation. The average water saturation at zones 4 and 2 ranges from 20 % to 30 % respectively. The hydrocarbon saturation is represented by considerable occurrences along the studied reservoir (zone 2and 4) where it varies between 70% and 80% at zones 2 and 4 respectively. the pay zone yield 14 ft and 10 ft within zones 2 and 4 respectively, indicating a good pay zone. The studied sandy intervals (zones 2 and 4) reflected high gaseous records during the well drilling (Fig. 9 and Table 1). On the other hand, the petrophysical characteristics of the diagnostic shaly carbonates facies intervals (zones 1 and 3) are represented by a bad character, where the wetted average of gross thickness, net pay thickness, effective porosity, water saturation and shale content are represented by 19 ft, 1 ft, 11 %, 39 % and 17 % respectively for Zone 1, and represented by 23 ft, 2 ft, 13 %, 44% and 23 % respectively for zone3 (Fig. 9 and Table 1).

Table 1: Wetted average petrophysical parameters of the studied sub divided zones of the Nukhul Formation (Lower Miocene) southern Gulf of Suez, Egypt.

Zone Name	Top (ft)	Bottom (ft)	Gross	Net	N/G	Av Phi	Av Sw	So	Av Vcl	Phi*H	PhiSo*H
Zone 1	5391	5410	19	1	0.053	0.11	0.39	0.61	0.17	0.11	0.07
Zone 2 (Reservoir)	5410	5426	16	14	0.875	0.19	0.31	0.69	0.04	2.7	1.88
Zone 3	5426	5449	23	2	0.087	0.13	0.44	0.56	0.23	0.26	0.15
Zone 4 (Reservoir)	5449	5460	11	10	0.909	0.20	0.21	0.79	0.05	2.01	1.6
All Zones	5391	5460	69	27	0.391	0.19	0.27	0.73	0.07	5.08	3.69

4. 3. The statistical analysis of petrophysical parameters

Based on the veracity of petrophysical parameters and microfacies analysis, the examined Nukhul Formation could be classified into two facies including four distinct zones indicated by discrete plotted point assemblages (Fig. 10 and 11, Table 2). As a result, the current study focuses on the sandy facies of Zones 2 and 4. The statistical analysis and modeling of the petrophysical characteristics might be accomplished by achieving the interrelationship of all petrophysical parameters as follows:

4. 3.1. Porosity (ϕ_e) – permeability (K) relationship

The Sandy facies interval (zones 2 and 4) have effective porosity ranging from 9 to 23% (average 18% in both zones). Permeability in zone 2 ranges from 15 md to 239 md (~111 md), whereas zone 4 varies from 5 md to 634 md (~246 md) (Table 2). The relation coefficient (R) between porosity and permeabilities in the studied section is ($R_{zone2} = 0.71$, zone 2) and ($R_{zone4} = 0.92$, zone 4), indicating a good relationship between them and emphasizing that the studied reservoir is not severed by excessive diagenetic processes and facies change, whereas it gave a bad relation in shaly carbonates facies ($R = 0.22$) (Figs. 10 B and 11). The produced histograms show that permeability values are permanent below 350 md (Fig. 12A). The porosity values (10 - 24%) within sandy facies interval (zones 2 and 4) indicate a a good reservoir (Fig. 12B). The following equations can be used to represent permeability as a function of porosity:

$$\phi_e = 0.0295\,Ln(K) + 0.0295\,, \qquad R_{zone2} = 0.71 \qquad (5)$$

$$\phi_e = 0.0301\,Ln(K) + 0.0376\,, \qquad R_{zone4} = 0.92 \qquad (6)$$

4.3.2. Porosity (ϕ_e) - volume of sand (V_s) relationship

The sandy facies rocks (zones 2 and 4) are characterized by high volume of sand reach to 65 % and 63% respectively comparison with the other shaly carbonates facies zones that reach to 1 % and 19%at zones 1 and 3 respectively (Fig 10 C, Table 2). There is a strong relationship tie porosity (ϕ_e) and volume of sand in the studied reservoir (zones 2 and 4) which appear clearly in the relation between them with the relation coefficient reach to ($R = 0.87$) and ($R = 0.91$) at zones2 and 4 respectively and expressed by the following equations;

$$\phi_e = 0.2108(V_s) + 0.062\,, \qquad R_{zone2} = 0.87 \qquad (7)$$

$$\phi_e = 0.3663(V_s) + 0.062\,, \qquad R_{zone4} = 0.87 \qquad (8)$$

Middle East J. Appl. Sci., 14(3): 353-371, 2024
EISSN: 2706 -7947 ISSN: 2077- 4613 *DOI: 10.36632/mejas/2024.14.3.28*

4.3.3. Porosity (ϕ_e) - hydrocarbon saturation (S_o) inter-relationship

The hydrocarbon saturation of the sandy facies reservoir (zones 2 and 4) ranges from 86 % to 94% (~91%, zone 2) and varies from 0.38 to 86 % (~74% at zone 4), (Table 2). The constructed cross plots reflected that the zone 2 more saturated with hydrocarbon and the hydrocarbon saturation increases by increasing the porosity with the relation coefficient between them equal ($R_{zone2} = 0.73$) and ($R_{zone4} = 0.96$) at zones2 and 4 respectively building this equations (Fig. 10 D);

$$\phi_e = 1.0772(S_o) + 0.7978\,, \qquad R_{zone2} = 0.73 \quad \text{..} \quad (9)$$

$$\phi_e = 0.286(S_o) + 0.0262\,, \qquad R_{zone4} = 0.96 \quad \text{...} \quad (10)$$

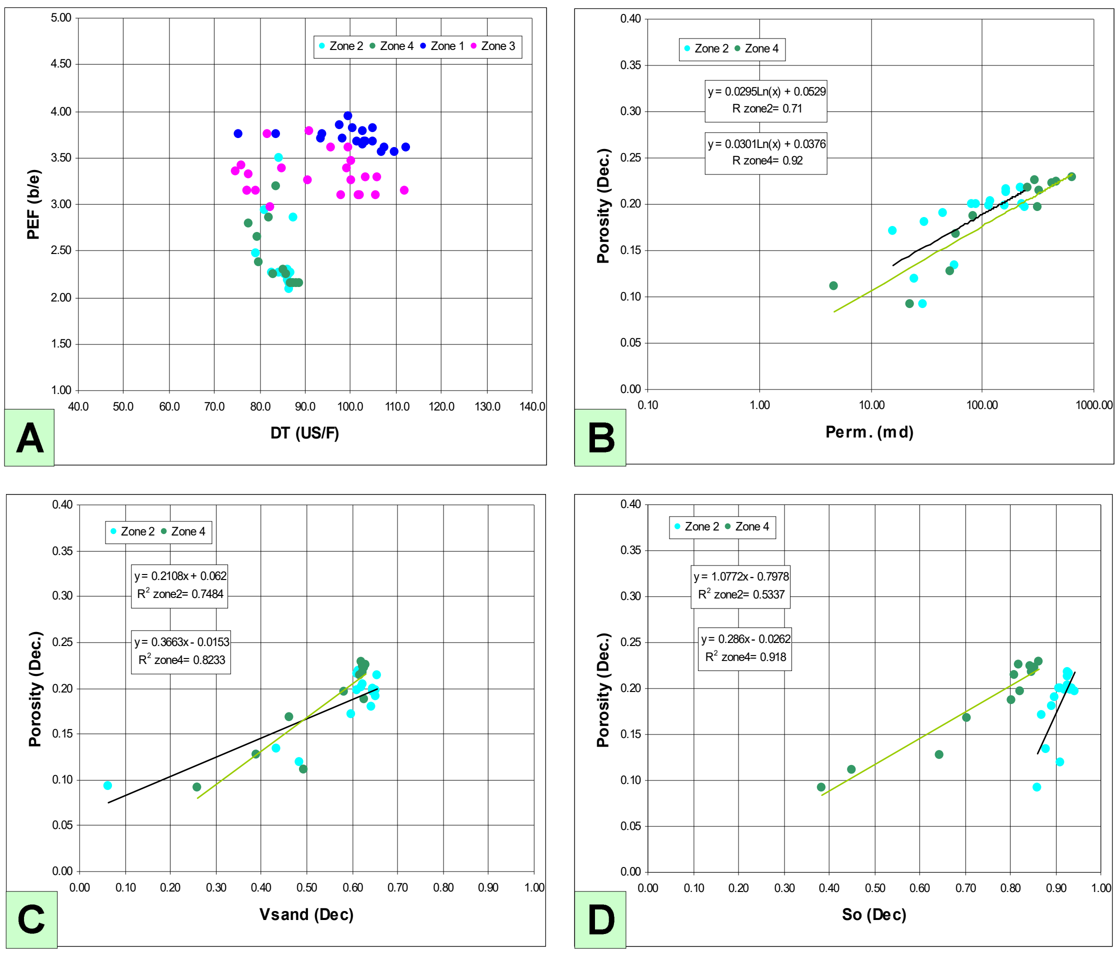

Fig. 10: The petrophysical parameters inter-relationship of the diagnostic reservoir intervals (zones 2 and4) A; plotting the sonic (DT, us/f) as a function of a photoelectric effect (PEF, b/e) representing the districted four zones of the Nukhul Formation, B; plotting the permeability (md) as a function of the effective porosity (Dec.), C; plotting the volume of sand as a function of the effective porosity (Dec.), D; plotting the hydrocarbon saturation as a function of the effective porosity (Dec.).

Middle East J. Appl. Sci., 14(3): 353-371, 2024
EISSN: 2706 -7947 ISSN: 2077- 4613 *DOI: 10.36632/mejas/2024.14.3.28*

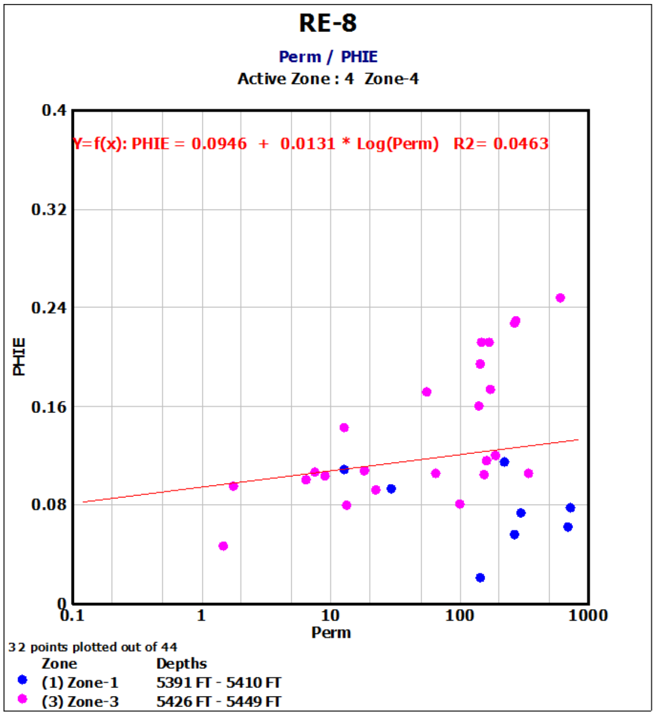

Fig. 11: Plotting the permeability (md) as a function of the porosity (Dec.) for non-reservoir rock units (zone 1 and3) in the study area, Southern Gulf of Suez, Egypt.

4.3.4. Porosity (ϕ_e) - Bulk density (ρ_b) relationship

The bulk density (ρ_b) for both shaly carbonates facies rocks type (zones 1 and 3) are ranged from 2.44 to 2.60 gm/cc with average 2.51 gm/cc. whereas the sandy facies type (zones 2 and 4) are ranged from 2.29 and 2.27 gm/cc to 2.57 and 2.50 gm/cc with an average reach to 2.36 and 2.35 gm/cc at zones 2 and 4 respectively (Table 2). The porosity increases by decreases the bulk density in the studied reservoir (zones 2 and 4) reflecting good correlation coefficients between them which are varies from ($R_{zone2} = 0.98$) and ($R_{zone4} = 0.99$) for the second and fourth zones respectively which yield mathematical equation models:

$$\phi_e = -0.4942(\rho_b) + 1.3482, \qquad R_{zone2} = 0.98 \quad (11)$$

$$\phi_e = -0.5826(\rho_b) + 1.5528, \qquad R_{zone4} = 0.99 \quad (12)$$

The petrographical analysis reveals that most of the analyzed rock samples are of low to moderate intra-granular porosity (Fig. 13A).

4.3.5. Porosity (ϕ_e) - volume of shale (V_{cl}) relationship

The shale volume is an effective factor that occluded the porosity, where this clearly appears in figure 13B. The shale volume (V_{cl}) of zones 2 and 4 ranges from 0.0 % to 32%, zone 2 and varies from 0.0 to 34 % at zone 4 (~ 8%) in both zones (Table 2). There is a strongly inversely relationship between porosity (ϕ_e) and shale volume of the sandy facies type (zones 2 and 4) with relation coefficients $R_{zone2} = 0.89$ (for zone 2) and $R_{zone4} = 0.91$ (for zone 4).

$$\phi_e = -0.3253(V_{cl}) + 0.2084, \qquad R_{zone2} = 0.89 \quad (13)$$

$$\phi_e = -0.4243(V_{cl}) + 0.2190, \qquad R_{zone4} = 0.91 \quad (14)$$

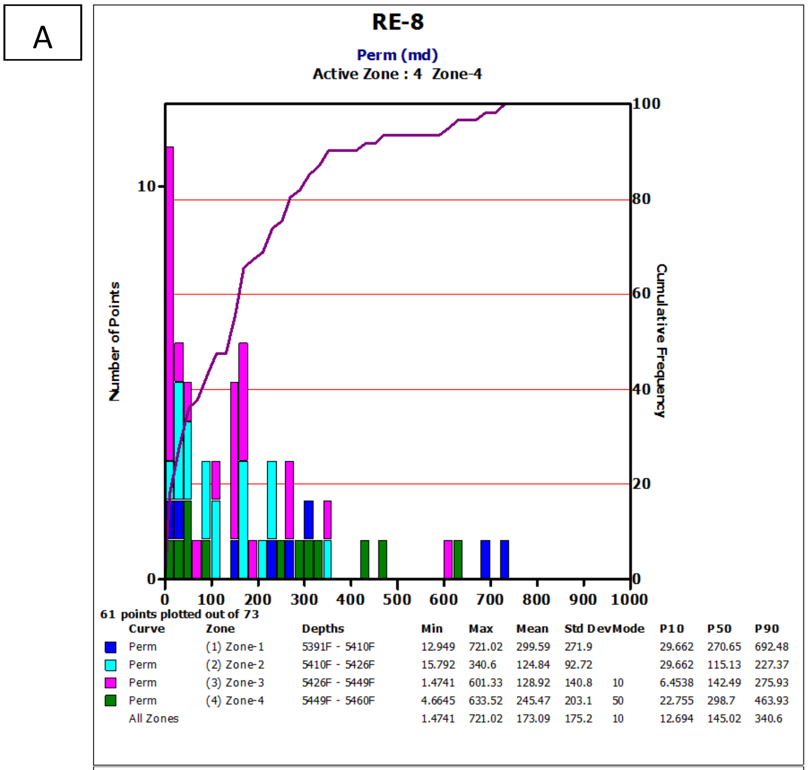

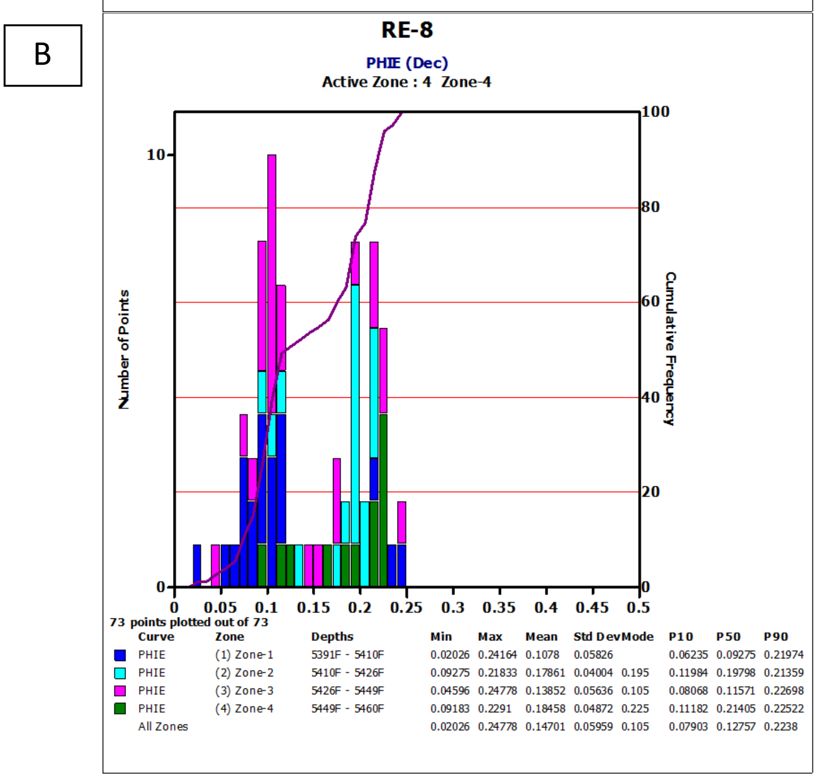

Fig. 12. A; Permeability histogram, B; Porosity histogram of the Nukhul reservoir, RE-8X well, Southern Gulf of Suez, Egypt.

4.3.6. Porosity (ϕ_e) – volume of lime (V_{lime}) relationship

The volume of lime (V_{lime}) of the sandy facies (zones 2 and 4) is very minor and ranges from 5 % to 21% (~ 12 %, zone2) and varies from 12 to 29 % (~ 17 % at zone 4, Table 2). The volume of lime has a differential effect on the porosity of the sandy facies, where it has a strong inversely relation with porosity ($R_{zone4} = 0.95$), at zone 4. At zone 2 it has a very low effect in the studied reservoir and this appear from the low relation coefficient ($R_{zone2} = 0.27$). This can be explained due to low volume of lime at zone 2 than that of zone 4 (Fig.13C).

$$\phi_e = -0.2377\,(V_{lime}) + 0.2115\,, \qquad R_{zone2} = 0.27 \quad \ldots(15)$$

$$\phi_e = -0.8482\,(V_{lime}) + 0.2115\,, \qquad R_{zone4} = 0.95 \quad \ldots(16)$$

4.3.7. Porosity (ϕ_e) – water saturation (S_w) inter-relationship

Zones 2 and 4 have significantly less water than non-reservoir zones (1 and 3). Zone 2 produces water saturations ranging from 6% to 14% (~9%) and 14 to 62% (~26% at zone 4). As a result, zone 4 is more impacted by water saturation than zone 2 (see Table 2). Water saturation blocked the linked porosity in the examined reservoir, particularly in zone 4, as evidenced by the relation coefficients of $R_{zone2} = 0.73$ and $R_{zone4} = 0.96$ for zones 2 and 4, respectively (Fig. 13D).

$$\phi_e = -1.0772\,(S_w) + 0.2794\,, \qquad R_{zone2} = 0.73 \quad \ldots(17)$$

$$\phi_e = -0.2860(S_w) + 0.2598\,, \qquad R_{zone4} = 0.96 \quad \ldots(18)$$

4.3.8. Porosity (ϕ_e) – photoelectric effect (PEF) inter-relationship

Schlumberger introduced the photoelectric factor (PEF) in the early 1980s as an additional tool to bulk measurements of density. PEF measurement is regarded an essential well logging technique for distinguishing between different types of reservoir rocks since it is sensitive to high-atomic-number elements. The photoelectric effect (PEF) is relatively of low value and has a good relation with porosity in both zones (2 and 4) of all reservoirs. The photoelectric effect (PEF) values of zone 2 ranges 2.09 to 3.5 b/e (~ 2.4 b/e) and varies from 2.15 to 3.2 b/e (~ 2.44 b/eat zone 4, Table 2). There is a strong inversely relation between porosity (ϕ_e) and the photoelectric effect within zones 2 and 4, with the relation coefficients r= 0.97 for zone 2, and r= 0.98 for zone 4 (Fig.13E).

$$\phi_e = -0.0926(PEF) + 0.405\,, \qquad R_{zone2} = 0.97 \quad \ldots(19)$$

$$\phi_e = -0.1355(PEF) + 0.515\,, \qquad R_{zone4} = 0.98 \quad \ldots(20)$$

Table 2: Statistical parameters of the petrophysical parameters of the studied zones of the Nukhul Formation, southern Gulf of Suez, Egypt.

		DT	NPHI	PEF	Perm.	PHIE	RHOB	SW	So	VCL	VDol	VLime	VS
		US/F	CFCF	b/e	md	Dec	G/C3	Dec	Dec.	Dec	dec	dec	dec
Zone 1	Av.	100.1	0.31	3.71	2181.7	0.11	2.50	0.36	0.64	0.48	0.18	0.23	0.00
	Min.	75.2	0.13	3.56	13	0.02	2.44	0.15	0.00	0.00	0.00	0.09	0.00
	Max.	112.3	0.37	3.94	9747.2	0.24	2.60	1.00	0.85	0.79	0.67	0.36	0.01
Zone 2	Av.	85.2	0.19	2.40	111.4	0.18	2.36	0.09	0.91	0.08	0.05	0.12	0.57
	Min.	79.2	0.16	2.09	15.8	0.09	2.29	0.06	0.86	0.00	0.00	0.05	0.06
	Max.	87.4	0.22	3.50	238.7	0.22	2.57	0.14	0.94	0.32	0.42	0.21	0.65
Zone 3	Av.	92.0	0.25	3.31	133.5	0.14	2.51	0.64	0.64	0.22	0.23	0.39	0.01
	Min.	74.7	0.11	2.97	1.5	0.05	2.44	0.12	0.12	0.00	0.00	0.00	0.00
	Max.	112.1	0.33	3.79	601.3	0.25	2.60	1.00	1.00	0.63	0.36	0.59	0.19
Zone 4	Av.	84.0	0.19	2.44	245.5	0.18	2.35	0.26	0.74	0.08	0.02	0.17	0.55
	Min.	77.5	0.14	2.15	4.7	0.09	2.27	0.14	0.38	0.00	0.00	0.12	0.26
	Max.	88.6	0.21	3.20	633.5	0.23	2.50	0.62	0.86	0.34	0.10	0.29	0.63

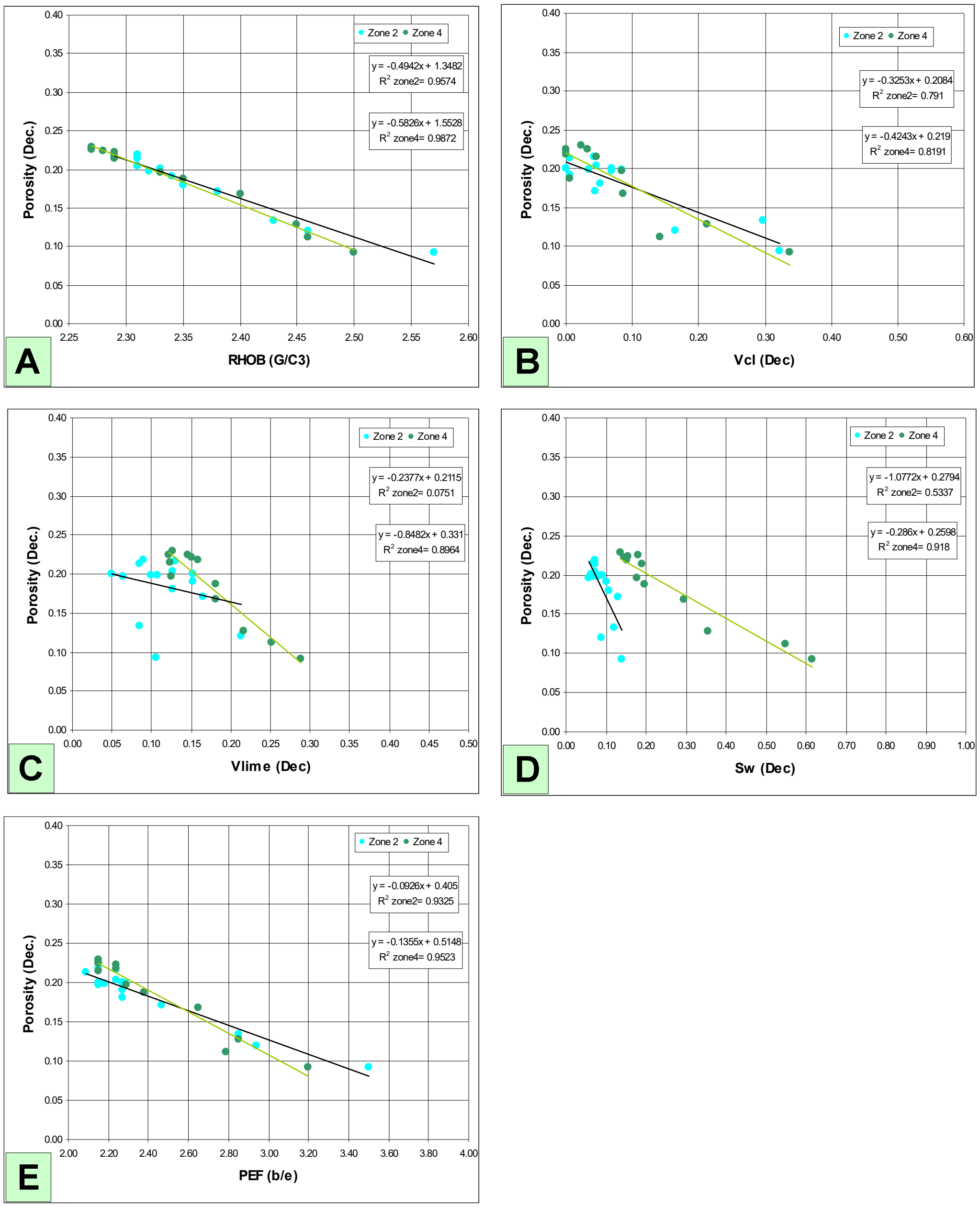

Fig. 13: The petrophysical parameters inter-relationship of the reservoir zones (zone 2 and4) A; Plotting the bulk density (G/C^3)as a function of effective porosity (Dec.), B; Plotting the clay volume (Dec.) as a function of theeffective porosity (Dec.), C; Plotting the volume of lime as a function of the effective porosity (Dec.), D; Plotting the water saturation (Dec.) as a function of theeffective porosity (Dec.), Plotting the photoelectric effect (PEF, b/e) as a function of the effective porosity.

5. Conclusion

The petrophysical analysis revealed that the oil net pay of the studied section is primarily concentrated in the sandy facies of zones 2 and 4, whereas the shaly carbonates facies facies (zones 1 and 3) are primarily composed of carbonates and shale rocks, with negligible oil occurrences acting as both cap and source rocks at the same time in the studied area. The rock and ditch samples revealed that the two sandy facies type (2 and 4) were colorless, yellow white, off white, loose, moderate to coarse grained, sub-angular to sub-round with calcareous cement, moderately sorted, and had good textural maturity. Furthermore, there is strong evidence of brown oil with a quick pale yellow stream cut, as well as a high recording of gas values in the opposing zones. According to the petrophysical model, the effective porosity of Nukhul Formation sandy facies type is primarily determined by the following parameters: permeability, sand volume, hydrocarbon saturation, bulk density, shale content, lime volume, water saturation, and photoelectric effect. The relationships between effective porosity and the other parameters for zones 2 and 4 were discussed. The electrical characteristics are influenced by lithology, porosity, and permeability. Petrography reveals that there are two kinds of lithology: sandstone and limestone, with some clay elements present in trace amounts

Acknowledgement

I would like to ensure the deep thanks to Al Azhar university and geophysical team of geophysical science department, National Research Center, Egypt and I would like to send a great thanks to Prof. Dr. Adel Othman in geology department, Al Azhar university for great helpful to establishing this work.

Conflict of Interest

Authors declare that they have no competing interests as defined by Springer, or other interests that might be perceived to influence the results and/or discussion reported in this paper.

Funding

"No funding was obtained for this study".

Competing interests

Authors declare any financial and non-financial competing interests in relation to this described work.

References

Abd El Aziz E.A., and M.M. Gomaa, 2022a. Electrical properties of sedimentary microfacies and depositional environment deduced from core analysis of the synriftsediments, Northwestern shore of Gulf of Suez, Egypt, J. of Petroleum Exploration and Production Technology, 12: 2915-2936.

Abd El Aziz, E.A., and M.M. Gomaa, 2022b. Petrophysical analysis of well logs and core samples for reservoir evaluation: a case study of Southern Issaran Field, Gulf of Suez province, Egypt. Environmental Earth Sciences (2022) 81:341. https://doi.org/10.1007/s12665-022-10420-x

Gomaa M.M., and E.A. Abd El Aziz, 2024. Depositional environment, petrophysical evaluation and electrical properties of Zeit Formation, Northwestern shore of Gulf of Suez, Egypt. Journal of Earth Science, in print.

Abd El Gawad E., N. Abd El Hafez, M.S. Hammed, and H.A. El Naggar, 2016, Characterization of pre-rift reservoirs of western Hurghada district, Egypt. Int. J. of Innov. Sci. Eng. Technol., 3 (12):74–83.

Abou El-Anwar E., and M.M. Gomaa, 2013, Electrical properties and geochemistry of carbonate rocks from the Qasr El-Sagha formation, El-Faiyum, Egypt, Geophysical Prospecting, 61: 630-644.

Abul-Nasr, R.A., 1990. Re-evaluation of the Upper Eocene rock units in west central Sinai, Egypt. Ain Shams University, Earth Science Series, 4: 234–247.

Alsharhan, A.S., 2003, Petroleum geology and potential hydrocarbon plays in the Gulf of Suez rift basin, Egypt. A.A.P.G., Bull. 87:143-180.

Archie, G.E., 1942, The electrical resistivity logs as an aid in determining some reservoir characteristics. Trans. AIME, 146: 54-62.

Bosworth, W. and K. McClay, 2001, Structural and stratigraphic evolution of the Gulf of Suez Rift, Egypt: a synthesis. In: Ziegler, P. A., Cavazza, W., Robertson, A. H. F., Crasquin-Soleau, S. (Eds.), Peri-Tethys Memoir 6: Peri-Tethyan Rift/Wrench Basins and Passive Margins, Mem. Mus. Natn. Hist. Nat., 186: 567-606.

Chowdhary, L.R., and S. Taha, 1987, Geology and habitat of oil in Ras Budran field, Gulf of Suez. Egypt AAPG Bull, 71(10):1274-1293.

Colleta, B., P. Le Quellec, J. Letouzey and I. Moretti, 1988, Longitudinal Evolution of the Suez rift structure, Egypt. Tectanophysics, 153: 221-233.

Corex, 2009, Special core analysis study, Issaran Field, Egypt. Internal reports.

Egyptian General Petroleum Corporation (EGPC), 1996. Gulf of Suez oil and gas fields, A comprehensive overview. Cairo, Egypt.

El Nady M.M., N.S. Mohamed, and A.N. Shahin, 2016, Source-rock potential of Miocene-Paleozeoic sediments in GH-376 oilfield, South Gulf of Suez Egypt. En Sour, Part A: Recover, Util, Environ. Eff. 38(1):100–109.

El-Ghali M.A.K., E. El Khoriby, H. Mansurbeg, S. Morad, and N. Ogle, 2013. Distribution of carbonate cements within depositional facies and sequence stratigraphic framework of shore face and deltaic arenites, lower Miocene, the Gulf of Suez rift, Egypt, Marine and Petroleum Geology.

Evans, A.L., 1990, Miocene sandstone provenance relations in the Gulf of Suez: insights into syn-rift unroofing and uplift history. AAPG Bull, 74:1386–1400.

Evans, A.L., 1988. Neogene tectonic and stratigraphic events in the Gulf of Suez Rift area, Egypt. Tectanophysics, 153: 235-247.

Garfunkel R.L. and Y. Bartov, 1977, The Tectonic of the Suez Rift: Geological Survey of Israel Bulletin, 71: 1-44.

Khalil, B., and W.M. Mesheref, 1988. Hydrocarbon occurrences and structural style of the southern Suez rift basin. In: Egypt 9thpetroleum exploration and production conference, EGPC, Cairo, Egypt, 1: 86–109.

Leila, M. and A. Moscariello, 2018. Depositional and petrophysical controls on the volumes of hydrocarbons trapped in the Messinian reservoirs, onshore Nile Delta, Egypt. Petroleum 4: 250-267.

McClay, K.R., G.J. Nichols, S.M. Khalil, M. Darwish, and W. Bosworth, 1998, Extensional tectonics and sedimentation, eastern Gulf of Suez, Egypt. In Sedimentation and tectonics in Rift Basins Red Sea: Gulf of Aden (223–238). Springer, Dordrecht.

Moustafa, A.R., 1997. Controls on the development and evolution of transfer zones: the influence of basement structure and sedimentary thickness in the Suez rift and Red Sea. Jour. of Structural Geology, 19: 755-768.

Moustafa, A.R., and S.M. Khalil, 2016, Control of extensional transfer zones on syn-tectonicand post-tectonic sedimentation: implications for hydrocarbon exploration, J. Geol.Soc., 174: 318–335.

Moustafa A.R., and S.M. Khalil, 2020, Structural setting and tectonic evolution of the Gulf of Suez, NW red sea and Gulf of Aqaba Rift systems. In: Hamimi Z, El-Barkooky A, Frias JM, Fritz H, El-Rahman YA (Eds) The geology of Egypt. Springer, Cham, 295–342.

Omar G.I., M.S. Steckler, W.R. Buck, and B.P. Kohn, 1989. Fission-track analysis of basement apatites at the western margin of the Gulf of Suez rift, Egypt: evidence for synchroneity of uplift and subsidence. Earth Planet Sci. Lett., 94:316–328.

Peijs, J.A.M.M., T.G. Bevan, and J.T. Piombino, 2012. The Gulf of Suez rift basin. In: Roberts, Bally (Eds.), Phanerozoic rift systems and sedimentary basins. Elsevier B.V., 165–194.

Pickett G.R., 1973. Pattern recognition as a mean of formation evaluation. Paper A in 14th Annual Logging symposium transactions: society of professional well log analysis, paper A, 1-21.

Radwan, A., and S. Sen, 2021. Stress path analysis for characterization of in situ stress state and effect of reservoir depletion on present-day stress magnitudes: reservoir geomechanical modeling in the Gulf of Suez Rift Basin Egypt. Nat. Resour. Res., 30(1):463–478.

Radwan A.E., 2021. Modeling pore pressure and fracture pressure using integrated well logging, drilling based interpretations and reservoir data in the giant El Morgan oil field, Gulf of Suez Egypt. J. Afr. Earth. Sci., 178:104165.

Radwan A.E., 2021b, Modeling the depositional environment of the sandstone reservoir in the middle miocenesidri member, badri field, Gulf of Suez Basin, Egypt: integration of gamma-ray log patterns and petrographic characteristics of lithology. Nat. Resour. Res. 30(1): 431–449.

Robson D.A., 1971. The structural of the Gulf of Suez clysmic rift with spcialspecial reference to the Eastern side. J. of Geological Society, 127: 247-276.

Said, R., 1990.The Geology of Egypt. E.G.P.C., CONOCO, Hurghada Inc. and Repsol. Expl. S.A., 734.

Sarhan M.A. and A. Basal, 2019. Ahmed basal Evaluation of Nubia sandstone reservoir as inferred from well logging data interpretation for Rabeh East-25 well, Southwest Gulf of suez, Egypt. J. African Earth Science, 155: 124-136.

Saoudi A, and B. Khalil, 1984, Distribution and hydrocarbon potential of Nukhul sediments in the Gulf of Suez. In: Proceedings of 7thpetroleum exploration and production conference, 75–96.

Saoudi, A., A.R. Moustafa, R.I. Farag, M.M. Omara, H. Wally, A. Fouad, A. Tag, and R.Z. Ragab, 2014. Dual-porosity fractured miocenesyn-rift dolomite reservoir in the Issaran Field (Gulf of Suez, Egypt): a case history of the zonal isolation of highly fractured water carrier bed Geological Society, London, Special Publications, 374, first published on September 5, 2012. https://doi.org/10.1144/ SP374.7.

Sarhan M.A., 2020, Geophysical appraisal and oil potential for Rudeis Formation at West Hurghada area, southern Gulf of Suez: detection of stratigraphic trap. Arab. J. Geosci. 13(6):1–9.

Sarhan M.A., 2021 Geophysical and hydrocarbon prospect evaluation of Nukhul Formation at Rabeh East oil field, Southern Gulf of Suez Basin, Egypt. Journal of Petroleum Exploration and Production Technology, 11: 2877–2890.

Schlumberger, 1972. Log Interpretation/Charts. Schlumberger Well Services Inc., Huston, 1, 113.

Schlumberger, 1984. log interpretation charts. schlumberger well services, U.S.A., 423.

Schlumberger, 1995. Well evaluation conference, Egypt. Paris, France, 87.

Schlumberger, 1998. Schlumberger log interpretation principle applications. Schlumberger educational services, Houston, Texas, 222.

Sellwood, B.W. and R.E. Netherwood, 1984, Facies evaluation of the Gulf of Suez area sedimentary history as indicator of rift initiation and development. Modern Geology, 9: 43-69.

Shaltout, A.A., M.M. Gomaa, and M. Wahbe, 2012, Utilization of standardless analysis algorithms using WDXRF and XRD for Egyptian Iron Ores identification. X-Ray Spectrometry, 41(3): 355–362.

Sherif, F., S. Souvik, B. Nancy, A. Mohammad, M. Ehab, and A. Mohammad, 2023. Assessment of the petrophysical properties and hydrocarbon potential of the Lower Miocene Nukhul Formation in the Abu Rudeis-Sidri Field, Gulf of Suez Basin, Egypt. Geomech. Geophys. Geo-energ. Georesour., 9: 36.

Sultan N., 2002. Gulf of Suez/Red Sea structural evaluation and hydrocarbon potentiality. In: International petroleum conference and exhibit, 82.

Temraz, M., and H. Dypvik, 2018. The lower MioceneNukhul Formation (Gulf of Suez, Egypt): microfacies and reservoir characteristics. J. Petrol. Explor. Prod. Technol., 8(1): 85–98.

Zaid, M., 2013. Provenance, diagenesis, tectonic setting and reservoir quality of the sandstones of the Kareem Formation, Gulf of Suez, Egypt. Journal of African Earth Sciences, 85: 31-52.